

Expanded secondary craters in the Arcadia Planitia region, Mars: Evidence for tens of Myr-old shallow subsurface ice



Donna Viola ^{a,*}, Alfred S. McEwen ^a, Colin M. Dundas ^b, Shane Byrne ^a

^aLunar and Planetary Laboratory, University of Arizona, Tucson, AZ 85721, USA

^bAstrogeology Science Center, U.S. Geological Survey, Flagstaff, AZ 86001, USA

ARTICLE INFO

Article history:

Received 8 June 2014

Revised 29 September 2014

Accepted 17 October 2014

Available online 25 October 2014

Keywords:

Ices

Impact processes

Mars, climate

Mars, surface

ABSTRACT

A range of observations indicates widespread subsurface ice throughout the mid and high latitudes of Mars in the form of both pore-filling and excess ice. It is generally thought that this ice was recently emplaced and is not older than a hundred thousand to a few millions of years old based on ice stability and orbital-induced climate change. We analyze the distribution of subsurface ice in Arcadia Planitia, located in the northern mid latitudes, by mapping thermokarstically expanded secondary craters, providing additional evidence for extensive excess ice down to fairly low latitudes (less than 40°N). We further infer the minimum age of this subsurface ice based on the ages of the four primary craters that are thought to be the source of a large portion of these secondaries, which yields estimates on the order of tens of millions of years old – much more ancient than anticipated. This estimated ancient age suggests that ice can be preserved in the shallow subsurface for long periods of time, at least in some parts of Arcadia Planitia where expanded secondary craters are especially abundant. We estimate the amount of ice lost to sublimation during crater expansion based on measurements of expanded secondary craters in HiRISE Digital Terrain Models. The loss is equivalent to a volume of ice between ~140 and 360 km³, which would correspond to a global layer of 1–2.5 mm thick. We further argue that much more ice (at least 6000 km³) is likely preserved beneath the un-cratered regions of Arcadia Planitia since significant loss of this excess ice would have caused extensive terrain dissection and the removal of the expanded secondary craters. Both the loss of ice due to secondary crater expansion and the presence of this ice today have implications for the martian climate.

© 2014 Elsevier Inc. All rights reserved.

1. Introduction

Evidence for widespread ground ice on Mars, particularly in the polar regions and mid latitudes, has been accumulating in recent years from a range of orbital observations. Morphological characteristics found throughout the northern martian mid latitudes suggest the presence of subsurface ice (reviewed by Carr, 1996). Mars Odyssey's Gamma Ray Spectrometer and Neutron Spectrometer have indicated the presence of ice that exceeds the regolith pore space, called "excess" ice, in the uppermost meter of the martian surface (e.g. Boynton et al., 2002; Feldman et al., 2004). Thermal inertia measured by Mars Global Surveyor's Thermal Emission Spectrometer (TES) indicates a buried ice-rich permafrost layer between 50° and 80°N at a depth of a few to tens of centimeters (Bandfield and Feldman, 2008), largely consistent with distribution

of ice detected by the Neutron Spectrometer. The Mars Advanced Radar for Subsurface and Ionosphere Sounding (MARSIS) on Mars Express, with a vertical resolution of 50–100 m (Picardi et al., 2004), has detected ice at the scale of decameters throughout the high latitudes of both hemispheres (e.g. Mouginot et al., 2010, 2012), and the Shallow Radar (SHARAD) instrument on the Mars Reconnaissance Orbiter (MRO) has confirmed that some mid-latitude lobate debris aprons, hundreds of meters thick, are mostly ice (Holt et al., 2008; Plaut et al., 2009). Also, polygonal-patterned ground, thought to form by thermal contraction cracking and indicative of subsurface ice, has been observed at a range of scales throughout the northern and southern middle and high latitudes on Mars (e.g. Mellon et al., 2009b; Levy et al., 2010). The Phoenix lander verified these inferences of widespread ground ice by directly excavating both pore-filling and nearly pure ice within centimeters of the surface (Smith et al., 2009; Mellon et al., 2009a). All of these observations are consistent with theoretical models which indicate that water ice should be stable in the martian subsurface poleward of ~45–60° (e.g., Leighton and Murray,

* Corresponding author at: 1629 E. University Blvd., Rm. 324, Tucson, AZ 85721, USA.

E-mail address: dviola@lpl.arizona.edu (D. Viola).

1966; Mellon et al., 2004; Chamberlain and Boynton, 2007; Schorghofer, 2007).

Pore-filling ice is thought to form by vapor deposition within porous soil, whereas excess ice likely forms as a result of thin films of water forming ice lenses (Mellon et al., 2009a; Sizemore et al., in press) or from buried snow (Head et al., 2005; Fastook et al., 2011), although Fisher (2005) proposed an alternative mechanism where temperature-driven thermal cracking and diffusive migration of water vapor can build a subsurface cryoshell over many seasonal temperature cycles. Recent work by Sizemore et al. (in press) indicates that ice lens initiation should be common at high martian latitudes, and that the rate of growth is most rapid in clay soils or in the presence of deliquescent salts like perchlorates, producing centimeters-thick layers of excess ice on timescales of hundreds to tens of thousands of years.

Excess ice has been noted in Utopia Planitia based on radar sounding (Stuurman et al., 2014) and high concentrations of periglacial, ice-related landforms, including polygonal-patterned ground and thermokarst-like depressions (Sejourne et al., 2012; Soare et al., 2012). Several lines of evidence also support the hypothesis of extensive subsurface ice, including excess ice, in and around Arcadia Planitia, a smooth Amazonian-age plain in the martian northern mid latitudes centered at 47°N, 184°E. These include widespread thermal contraction polygons (Barrett et al., 2013), neutron measurements from Mars Odyssey (Feldman et al., 2011), an abundance of pedestal craters, discussed below (Kadish et al., 2009), and the presence of terraced craters thought to result from impacts into icy layered targets (Bramson et al., 2013).

Impact craters can act as “windows” to provide context for subsurface properties such as layering and the presence/abundance of volatiles, including water ice. Clean ice has been exposed by several small, recently-formed primary craters as far equatorward as 39°N (Byrne et al., 2009; Dundas et al., 2014a), demonstrating that near-surface excess ice is present today. Models of the observed sublimation from these ice exposures imply that the subsurface ice layer is relatively pure, perhaps overlying pore-filling ice-rich regolith (Dundas and Byrne, 2010; Kossacki et al., 2011), although the depth, thickness, and composition (in terms of fractional dust content and porosity) of the subsurface ice layer are not well constrained.

Furthermore, certain impact ejecta morphologies on Mars have been shown to correlate with latitude, and presumably subsurface ice content. In particular, the double- and multiple-layered ejecta types associated with the primary craters we will discuss in this study tend to be found in regions where ground ice is predicted to be stable (Mouginis-Mark, 1981; Barlow and Bradley, 1990), and it has been argued that ground ice is involved in their formation (e.g. Barlow, 2005). Excess ejecta craters, perched craters, and pedestal craters also tend to be found in ice-rich regions, where it is hypothesized that excess ice is preserved beneath either a thin surface lag (for pedestal craters) or rocky ejecta material excavated from beneath an icy subsurface layer (for excess ejecta and perched craters) (Kadish and Head, 2011); however, there are some interpretations of SHARAD data that suggests pedestal craters may be less ice-rich than previously thought, possibly comprised of a mix of ice and silicates (Nunes et al., 2011). Models simulating impacts into icy terrains provide an additional, theoretical basis for some of the unusual crater morphologies that we observe on Mars, and imply that Mars’ cratering record reflects the planet’s climatic history (Senft and Stewart, 2008).

Secondary craters, which form when material is ejected and re-impacts the surface, can also give an indication of subsurface properties. They are typically found in rays or clusters of small craters that emanate from the primary (source) impact crater, and may, if sufficiently well preserved, have herringbone patterns due to

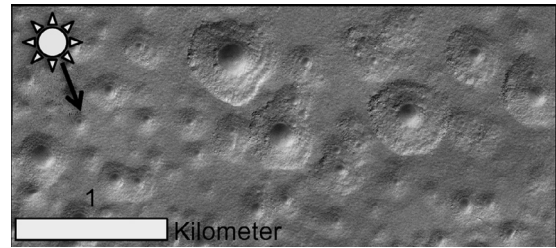


Fig. 1. Examples of expanded secondary craters, ESP_028411_2330, located near 52.7°N, 216.3°E.

interacting ejecta (Oberbeck and Morrison, 1973; Melosh, 1989). Secondaries can become difficult to distinguish from small primary craters at large distances from their source impact. Secondary craters can be very useful probes of target properties because large numbers of secondaries form nearly simultaneously (e.g. McEwen et al., 2005). Since the time for degradation to occur is identical, different secondary crater morphologies within a given secondary crater field can indicate variations in surface and subsurface conditions that can be explored over large spatial extents. Secondary crater fields appear to be rare at higher latitudes on Mars (Boyce and Mouginis-Mark, 2006), perhaps related to sublimation of ice (Weiss and Head, 2013). Arcadia Planitia is the exception, where we have found four craters with diameters ranging from 6 to 20 km, all with well-preserved secondaries. Many of these secondaries have “expanded” morphologies (Dundas et al., 2014b, submitted for publication), where the initial crater appears to have developed a shallow extension (Fig. 1). Although expanded craters have not been extensively studied previously and there has not been a systematic survey of these types of features, they appear concentrated near Arcadia Planitia, and a few isolated instances have been observed at high latitudes in other parts of the northern and southern hemispheres, including in Hellas basin (e.g. HiRISE images ESP_032463_1275, ESP_034931_1350). Kostama et al. (2006) previously identified these features as mantled pits in images taken by the Mars Orbiter Camera (MOC), and interpreted them as related to local geology. However, with our analysis of broader coverage using MRO’s Context Camera (CTX), we can see that these pits can be radially associated with the primary craters mentioned above, suggesting that they are in fact modified secondary craters. Fig. 2 compares a cluster of expanded secondaries from Domoni crater to a cluster of Zunil secondaries at a similar distance from the respective primary craters, demonstrating this radial association. We argue that these secondary craters were modified over time by a mechanism similar to terrestrial thermokarst, although in the martian case, water ice is sublimated instead of melted. Thermokarstic crater expansion involves the sublimation of relatively-clean subsurface ice exposed during impact events, a process which has been demonstrated by thermal and landscape evolution modeling (Dundas et al., submitted for publication). This expansion requires the presence of “excess ice” exceeding the natural pore space of the soil, involving the collapse of material overlying such an ice-rich layer as the unstable near-surface ice sublimates, and likely ceases when a sufficient lag has developed above the ice to prevent further sublimation. Therefore, we suggest here that the distribution and minimum age of subsurface excess ice near Arcadia Planitia can be broadly constrained by mapping the secondary crater fields of several well-preserved primary craters in the region.

2. Expanded crater formation mechanism

Fig. 3 shows an expanded secondary crater typical of the ones seen in Arcadia Planitia next to an unrelated crater, likely primary

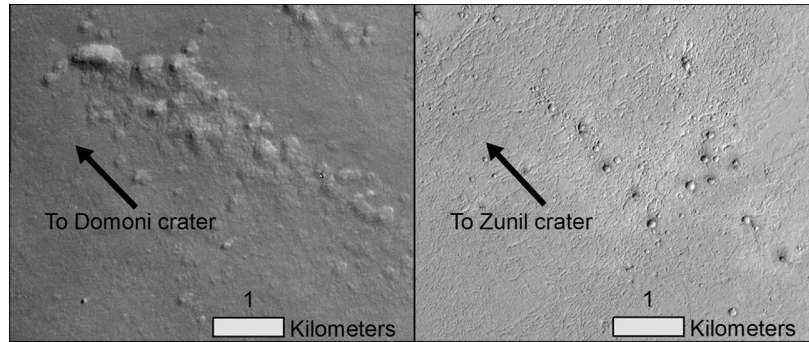


Fig. 2. Secondary craters from Domoni crater (left) and Zunil crater (right), both at a distance of ~ 130 km from their source primary. Note that expansion can be seen in some of the Domoni secondaries (and that some appear to have degraded beyond the appearance of craters), whereas the Zunil secondaries have crisp edges with no sign of expansion.

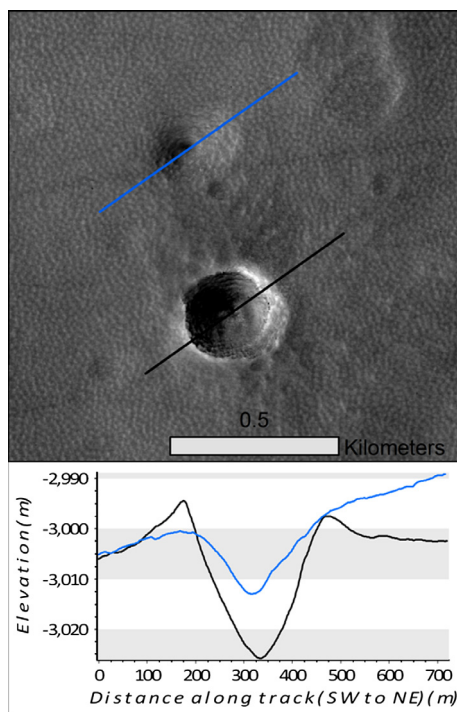


Fig. 3. The typical elevation profile of an expanded (secondary) crater (blue), compared to a primary crater (black) with a similar diameter measured in a HiRISE Digital Terrain Model (DTM). Note that the expanded crater is shallower with a more cone-shaped morphology, and does not show any evidence for a crater rim. Slight kinks in the slope indicate steepening at the central cavity of the expanded crater (HiRISE DTM DTEEC_018046_2375_017822_2325). (For interpretation of the references to color in this figure legend, the reader is referred to the web version of this article.)

but possibly a distant, lone secondary crater from a more recent impact. These two craters have comparable diameters (~ 0.25 km), but their elevation profiles, extracted from HiRISE stereo data, are different (Fig. 3). Note that the primary crater is deeper and has a very apparent rim, whereas the expanded crater is shallow and tapers off to the surface in line with an overall SW-to-NE upward slope, and the inner crater slopes steepen into a central depression. A larger-scale slope from NW to SE is responsible for the difference between the elevations at the northeastern end of each profile. The models of Dundas et al. (2014b) found that the best fit for typical observed expanded crater profiles was one where a crater penetrated into or through a pure ice layer, and the timescale for expansion was a minimum of a few tens of

thousands of years (Dundas et al., submitted for publication). Aeolian modification can affect crater morphologies, but is unlikely, by itself, to produce the expanded profiles that we observe. Impacts into layered targets may have some morphological similarities to expanded craters, but the elevation profiles (Bramson et al., 2013) and formation mechanisms of these types of craters are distinct. Craters that impact into layered targets typically develop more discrete terrace levels, which form at the time of impact due to the responses of different target materials to the shock wave. Since fresh, un-expanded craters can be found adjacent to expanded craters (Fig. 3), this is an unlikely formation mechanism for the expanded crater morphologies discussed here. It is possible that younger craters are in the process of slowly expanding at a scale that we cannot resolve in the available data, but the expanded morphology does not occur at the time of impact. Therefore, we interpret the mechanism responsible for crater expansion as sublimation-thermokarst and associated with a near-surface layer of relatively pure ice.

3. Objectives

The primary objective of this study is to better understand the distribution, history, and origin of subsurface ice in Arcadia Planitia by mapping expanded secondary craters. Because secondary craters and their source craters form nearly simultaneously, we can derive estimates of the age of the secondary craters, and thus of the minimum age of the ice layer into which they impacted. Mapping was done using images from the Context Camera (CTX; Malin et al., 2007) on MRO. The use of high-resolution imagery (~ 6 m/pixel) allowed for mapping clusters of secondary craters with diameters on the order of several decameters, and since 75% of the region was covered by CTX, we were able to acquire a detailed understanding of the distribution of secondary craters throughout Arcadia Planitia and the nearby areas.

We also estimate how much ice was lost during the expansion of these craters by investigating the three-dimensional structure of these features in seven Digital Terrain Models (DTMs) produced from stereo images taken by MRO's High Resolution Imaging Science Experiment (HiRISE; McEwen et al., 2007) using the methods described by Kirk et al. (2008), and extrapolating the estimates of ice loss in specific regions across the entire Arcadia Planitia study area.

4. Study region

The study area is between $35\text{--}65^\circ\text{N}$ and $180\text{--}240^\circ\text{E}$ (Fig. 4), including most of Arcadia Planitia as well as adjacent terrain. Within this area, there are four primary craters with well-preserved

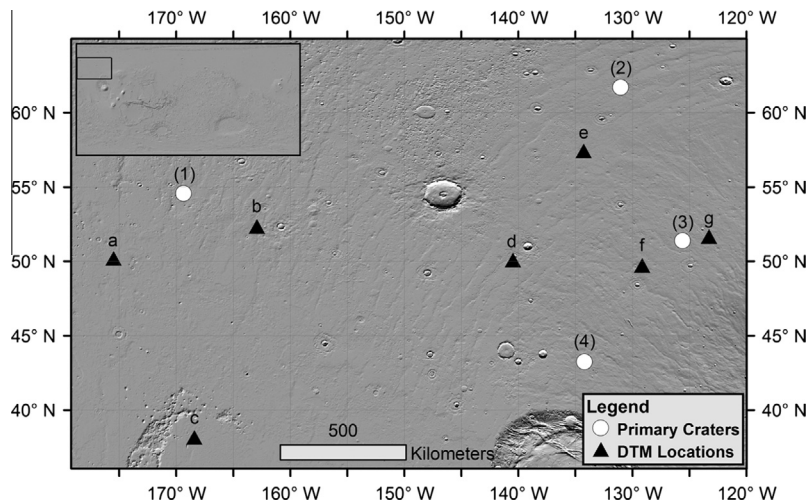


Fig. 4. MOLA shaded relief map of Arcadia Planitia study area (inset at top left shows global context). White circles show the locations of 4 primary impact craters with well-preserved secondary crater fields (Table 1). Black triangles are HiRISE DTMs that contain expanded secondary craters (Table 2).

Table 1
Parameters of study primary craters.

| | Primary crater | Latitude | Longitude | Diameter (km) | Depth (m) | d/D | Geologic context (Skinner et al., 2006) |
|-----|------------------------------|----------|-----------|---------------|-----------|--------|--|
| (1) | Steinheim | 54.57°N | 190.65°E | 11.3 | 600 | 0.053 | Arcadia Formation (member 1); near edges of Arcadia Formation (member 3) and Vastitas Borealis (ridged and knobby members) |
| (2) | Gan | 61.7°N | 229.0°E | 19.3 | 900 | 0.0466 | Arcadia Formation (member 1) |
| (3) | Domoni | 51.4°N | 234.4°E | 13.82 | 800 | 0.058 | Alba Patera Formation (lower member) |
| (4) | Unnamed ("Crater α ") | 43.2°N | 225.8°E | 6 | 700 | 0.117 | Alba Patera Formation (lower member); near edge of Arcadia Formation (member 3) |

secondary crater fields, summarized in Table 1. With the exception of two craters on the south polar layered deposits (Schaller et al., 2005), secondary crater fields appear uncommon at high latitudes, possibly due to periglacial processes erasing smaller craters. The reason why secondary crater fields are preserved here and not elsewhere is unclear, but since many Arcadia Planitia secondary craters show evidence for sublimation expansion that ceases once a sufficient lag deposit has developed, it may be related to the abundance and persistence of preserved excess ice.

The primary craters that we focus on have diameters ranging from 6 to 20 km, and are found between 43° and 62°N (Table 1). Domoni crater is a multiple-layer ejecta (MLE) crater with a central pit, and has been further studied using a HiRISE DTM created from three overlapping pairs of stereo images. Steinheim crater is a double-layer ejecta (DLE) crater with a central peak of diameter 2.8 km, and a previous detailed analysis of the crater's ejecta and central peak suggest that the impact angle was fairly steep ($>45^\circ$) (Pietrek et al., 2013). The largest primary crater in this study, with a diameter of 19.3 km, is Gan crater, a double-layer ejecta summit pit crater. The secondary crater field of this primary has previously been described by Robbins and Hynek (2011), who observed highly-linear chains of craters using data from the Thermal Emission Imaging System (THEMIS) on Mars Odyssey and posited that the impact direction was from the southeast based on mapping the near-field secondary craters using eleven mosaicked CTX images. The fourth and smallest primary in this study, unnamed and henceforth referred to as Crater α , is a simple, double-layer ejecta crater 6 km in diameter. The depth-to-diameter (d/D) ratios for all of the complex primary craters (Table 1), while smaller than the commonly-accepted values for fresh craters of their respective diameters (Pike, 1980; Garvin and Frawley, 1998), are consistent with the shallower profiles expected for

craters of their diameters at high latitudes (Mouginis-Mark and Hayashi, 1993; Stepinski et al., 2009; Robbins and Hynek, 2012). Two smaller primary craters ($D = 1.94$ km at 50.19°N, 184.49°E, and $D = 3.15$ km at 60.23°N, 236.27°E) with secondary fields extending several crater radii from their primaries were also identified in this study, although they only cover a small part of the total study area.

Table 2 describes the seven HiRISE DTMs containing expanded secondary craters, which we use to topographically characterize these features. Many are concentrated near $\sim 50^\circ$ N, although there is one significantly farther north (57°N) and one significantly farther south ($\sim 38^\circ$ N). Between 14 and 200 expanded craters were measured in each DTM. In many cases it is challenging to determine from which primary crater each set of expanded secondary craters originated.

4.1. Geologic context

The geologic context (from Skinner et al., 2006) in the immediate vicinity of each primary crater is described in Table 1. The secondary crater fields associated with these primary craters are largely concentrated within member 1 of the Arcadia Formation (Aa1), which is associated with Amazonian-age lava flows, and the lower member of what Skinner et al. (2006) mapped as the Alba Patera Formation (Hal), the oldest and least distinct flows originating from Alba Mons during the late Hesperian/early Amazonian. There are also secondaries extending into other units of the Arcadia Formation (Aa 2–5) and Vastitas Borealis (ridged member, Hvr, and grooved member, Hvg), and overlying the older ejecta surrounding Milankovič crater (54.7°N, 213.3°E). Although the distribution of secondary craters is inherently non-uniform, expanded and apparently non-expanded secondary craters are

Table 2
HiRISE DTMs containing expanded secondary craters.

| HiRISE stereo pair | Center latitude | Center longitude | # Expanded craters measured |
|---------------------------------------|-----------------|------------------|-----------------------------|
| a ESP_025366_2305 and ESP_025498_2305 | 50N | 185.5E | 14 |
| b ESP_027027_2325 and ESP_027370_2325 | 52N | 197E | 24 |
| c ESP_025735_2185 and ESP_025801_2185 | 38N | 192E | 15 |
| d ESP_027158_2305 and ESP_026446_2305 | 50N | 220E | 197 |
| e ESP_018046_2375 and ESP_017822_2375 | 57N | 231E | 86 |
| f ESP_017413_2300 and ESP_017334_2300 | 49.5N | 231E | 39 |
| g ESP_026076_2320 and ESP_026419_2320 | 52N | 237E | 37 |

Table 3
Age estimates of primary craters from superposed crater counts.

| Primary crater | Age (est., Ma) | # Craters (superposed) | Diameter range (km) | Area (km ²) |
|-----------------|----------------|------------------------|---------------------|-------------------------|
| Gan | 70 ± 10 | 45 | 0.1–2.1 | 2370 |
| Crater α | 24.3 ± 5.5 | 19 | .08–.17 | 189 |
| Steinheim | 18.6 ± 3.2 | 34 | .08–.291 | 616 |
| Domoni | 19.2 ± 5.3 | 13 | .1–.2 | 562 |

sometimes found in fairly close association, suggesting a heterogeneous distribution of excess ice. It should be noted that small landforms that might indicate subsurface ice are not resolved at the scale of the broader geologic mapping and are likely to relate to more recent surface processes.

4.2. Crater statistics

Using the Hartmann (2005) production function for Mars over the map area of 3.3×10^6 km², we found that the time for four primary craters of this size to accumulate is expected to be $\sim 37_{-18}^{+29}$ Myr. Assuming these are all of the youngest craters larger than 5.66 km in this region, we expect that their formation dates spanned this interval. This is a rough estimate due to the small number of craters, but is consistent (within a factor of two) with ages from superimposed small craters described below and serves as a check on those ages. The age of each individual primary crater was estimated from counts of small, superimposed craters, the results of which are summarized in Table 3. Crater-retention ages ranged from 18.6 to 70 Ma from crater counts over the area of each primary crater and its continuous ejecta, with the exception of Domoni crater, where we excluded the interior of the crater due to extensive pitting on the crater floor. These may be lower limits on the primary crater ages because many processes erase small craters. Regardless, both approaches suggest that these four craters and their secondaries formed tens of millions of years ago. We observe clusters of expanded secondaries that can be radially associated with each of the 4 primary craters of interest, which implies that the excess ice that the secondary craters exposed is also tens of millions of years old and has survived the climate variations that have occurred since formation.

5. Mapping secondary crater fields

Mapping of secondary craters was done using ESRI's ArcGIS; a total of nearly 500 CTX images were mapped, covering an area of ~ 3 million km². Clusters of expanded and “normal” (non-expanded) craters were delineated, their secondary origin apparent due to their clustered nature and similar degradation states; locations where secondaries with both expanded and non-expanded morphologies were found in close association, typically

where the smaller craters had not been expanded, were denoted as “mixed” clusters. The secondary craters immediately surrounding each primary (within several crater radii) can be clearly associated with their source impact; however, at greater distances from the primary craters, the crater fields overlap and it becomes challenging to distinguish their origin. In some instances clusters that appear non-expanded at CTX resolution actually appear to have undergone a lesser degree of expansion in higher-resolution HiRISE images, so it is important to note that the classification of “normal” clusters only applies to their appearance at CTX resolution. An additional complication is that most likely some of the secondary craters that we identify originated from impacts other than the four study primaries. Although no other obvious large ($D > 4$ km), well-preserved primaries with secondary crater fields were identified within the bounds of the study area, one particular section in the southeastern-most extent of the region contains expanded secondaries that are radial to and might have originated from Tooting crater (23.1°N, 207.1°E), a young primary crater previously dated at < 2 Ma (Mouginis-Mark and Garbeil, 2007). These clusters of secondaries are more than 1000 km northwest of Tooting crater, whose secondary crater field has previously been mapped out to 540 km and appears to be asymmetrical and more concentrated northeast of the crater (Mouginis-Mark and Boyce, 2012). Therefore, it is conceivable that other distant secondary craters from unrelated impact events are included in our dataset. Nevertheless, it is not necessary to definitively identify the source impact to use expanded secondaries as indicators of the spatial extent of excess subsurface ice. It is also possible for primary impact events to create small clusters, or elongated chains in the case of an oblique entry, but many of the larger and highly elongated clusters are most likely secondaries (Popova et al., 2007).

We further noted the locations of non-clustered, expanded craters that we interpret to be secondaries based on their relative proximity to other craters with similar apparent degrees of expansion/degradation (and therefore, presumably the same formation time). However, it is likely that some of these are small primaries that formed under similar conditions as these secondary craters and underwent similar expansion processes. This possible mixing has no effect on our conclusions.

We found that approximately 3% of the total mapped area was heterogeneously covered by clusters of secondary craters, 50% of which contained apparent expanded morphologies at CTX resolution (Fig. 5). Secondary craters within a few crater radii of each primary impact largely tend to have normal, non-expanded morphologies at CTX resolution, whereas more distant secondaries appear to have undergone expansion.

A total of $> 17,000$ clusters with areas ranging from 0.03–1600 km² (median ~ 2 km²) were mapped, along with 75,000 isolated expanded craters. In order to estimate the total number of secondary craters within the clusters, the study area was divided into 100 km by 100 km grids, and the number of craters within a sample of clusters of each type (non-expanded, mixed, and expanded) per grid unit were counted to estimate the number of craters per km². These crater densities were extrapolated to the clusters within each grid using the cluster surface area to approximate the total number of craters in each cluster. The mapping and counting methods used account for most secondaries with diameters > 50 m (> 8 CTX pixels), and the approximate number of secondary craters that meet this criterion within the mapped study area is estimated to be $> 10^6$. It is important to note that this only includes the secondary craters within the area covered by CTX; given the heterogeneous nature of the secondary crater distribution, we do not extrapolate the number of secondary craters within the 25% of the study region that had not been covered by high-resolution imagery as of mid 2013. This uncertainty is irrelevant to the order-of-magnitude nature of our conclusions. Of the mapped

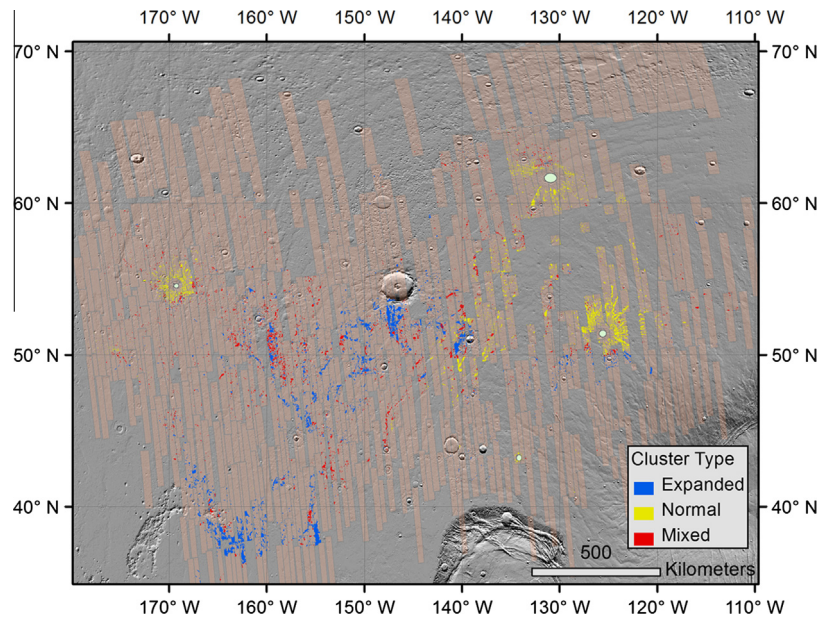


Fig. 5. Map showing CTX coverage (orange footprints) within the Arcadia Planitia study area, along with mapped secondary crater clusters. Colors denote clusters of non-expanded craters (yellow), expanded craters (blue), and a mix of the two (red).

area, 36% of the total number of secondaries were expanded, compared to ~45% with normal morphologies (and ~19% found in mixed clusters), even though the total areal extent of expanded secondaries is larger than that of non-expanded secondaries. This reflects the marked difference in the average crater density within clusters of each type; non-expanded clusters tend to contain the most craters per area, with an average of 11.9/km². Mixed clusters have an intermediate average density of 7.1/km², and expanded clusters contain the fewest craters per area, with 5.5/km². However, expanded craters also tend to be larger than apparently non-expanded craters, and the decreased crater density may be the result of crater expansion merging with or erasing smaller associated secondaries, perhaps ones that were too small to expand themselves or which have expanded beyond recognition since the time of their formation.

Few secondary craters, expanded or otherwise, are found at latitudes greater than ~65°N. Even in the case of Gan crater at 62°N, the concentration of secondary craters drops off rapidly towards more northern latitudes. This may be because periglacial processes such as thermal contraction polygons have been modifying the surface throughout recent climatic history, and remain active to the present day (Mellon et al., 2008), although polygonal ground is also found throughout the mid latitudes. An alternative possibility is that ice or atmospheric dust is deposited more frequently at higher latitudes, effectively erasing craters from the terrain. Note that all craters become rare at such high latitudes over Mars, so they must be actively erased (Korteniemi and Kreslavsky, 2013).

Another trend evident in the data is a correlation between expanded secondary craters and higher-standing ejecta associated with older, pre-existing impact craters. Although only about 9% of the mapped area is on or immediately surrounding the ejecta of older craters (including the large expanse around Milankovič crater), 40% of the total area of expanded secondary crater clusters (and 55% of the total number of expanded secondary craters) mapped in Arcadia Planitia are found associated with these materials. One reason for this trend may be that excess ice had been preferentially preserved beneath older craters and/or their ejecta as described by Kadish and Head (2011); MOLA elevation profiles of older craters with overlying expanded secondaries reveals that about half are either perched or pedestal craters, and therefore

may have preserved an ancient icy mantle layer (Meresse et al., 2006; Kadish and Barlow, 2006). However, this does not account for the expanded secondary craters found on other crater types, within excavated crater cavities, or in other parts of the northern plains. An alternate possibility is that crater ejecta and interiors either trap snow (e.g., due to surface roughness) or are favorable locations for ice lens growth (strongly dependent on regolith properties; Sizemore et al., in press).

5.1. Domoni crater

5.1.1. Volume of ejected material

We have acquired a constraint on the volume of material responsible for the formation of the Domoni crater secondaries using a DTM created from six HiRISE images of the impact crater (ESP_016846_2320, ESP_016569_2320, ESP_016213_2315, ESP_016714_2315, ESP_016780_2315, and ESP_016490_2315). The total rim-to-floor volume was 81 km³, and the volume of excavated material and the ejecta blanket were estimated using a MOLA interpolation of a pre-impact surface based on the topography outside the ejecta blanket. The respective ejecta and excavated volumes were 53.9 km³ and 60.6 km³, corresponding to a $V_{\text{ejecta}}/V_{\text{cavity}}$ ratio of 0.88, which is consistent with MOLA observations of martian impact craters (Garvin and Frawley, 1998). If the entirety of the volume deficit in the ejecta contributes to the production of the observed secondary crater field, it would suggest that approximately 7 km³ of material contributed to the production of the observed secondary craters. However, this order-of-magnitude estimate is complicated by material compression and escape during impact, post-impact surface rebound, and the likely ice-rich nature of the surface that would have resulted in vaporization during impact and sublimation shortly afterwards.

5.1.2. Size–frequency distribution

Two radial regions of secondary craters emanating from Domoni crater were selected, only one of which contained secondaries that underwent expansion (Fig. 6). Secondary crater diameters were measured (outer diameters in the case of expanded craters) wherever there was CTX coverage along each 140-km long, 2-km wide track, and the size–frequency distributions (SFDs) were

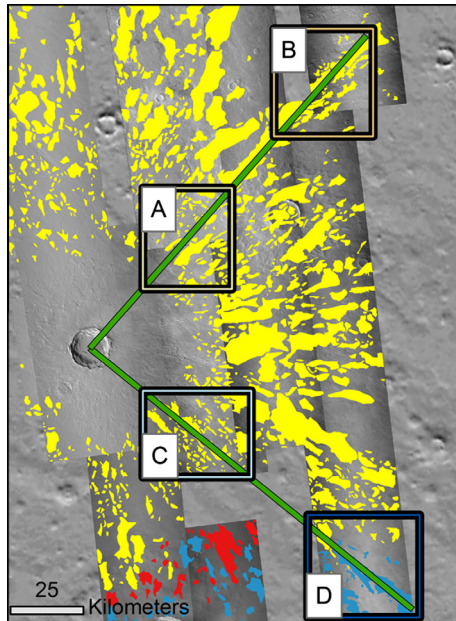


Fig. 6. Domoni crater and nearby secondary craters. Green tracks are 140-km long and 2-km wide, within which secondary crater size–frequency distributions were measured. Inner and outer regions of each track are enclosed in black boxes.

compared. Along the northeastern track, 2637 secondary craters with diameters ranging from 35 to 425 m were measured, and 1380 secondaries with diameters from 45 to 500 m were measured along the southeastern track. The innermost parts of both tracks, being close to the primary crater, did not show evidence for expansion as previously mentioned, so each track was split into the inner and outer regions shown in Fig. 6, where the outer regions contained Domoni secondary craters that were either expanded (in the southeast track) or non-expanded (in the northeast track). In both tracks, the inner region extended from the edge of Domoni crater’s continuous ejecta to ~ 80 km from the crater center and the outer region extended from ~ 100 to 140 km from the center of the crater. Fig. 7 shows the size–frequency distributions for this dataset, where the secondary craters in each surveyed region (within the green tracks in Fig. 6) were binned in multiplicative intervals of $2^{1/2}D$. Size–frequency distributions over small size ranges typically follow a power law trend of the form $N_{\text{inc}} = kD^{-b}$, where N_{inc} is the incremental number of craters, D is crater diameter, k is a constant, and b is the slope of the size–frequency distribution. There is a sharp drop-off in the incremental crater frequency at smaller diameters, but this can be attributed to resolution limits and the erasure of smaller craters through periglacial and aeolian processes. Some of the regions have SFDs that follow the power law described above (Fig. 7); however, the size–frequency distribution of the region containing expanded craters (region D in Fig. 6) appears nonlinear, with a parabolic shape in log space, and the SFD of the innermost region of the northeast track (region A in Fig. 6) does not strongly follow a power law trend. Table 4 shows the equations to describe the size–frequency distribution of each region. The slopes for the power law size–frequency distribution tend to increase with increasing distance from the primary crater, but all have a value of b between 3 and 5, which is typical for secondary craters on planetary bodies (McEwen and Bierhaus, 2006, and references therein). The SFD for the region containing expanded secondaries is shifted towards larger diameters relative to the outer non-expanded region, which is expected since we can only measure expanded diameters rather than the original diameters at the time of formation.

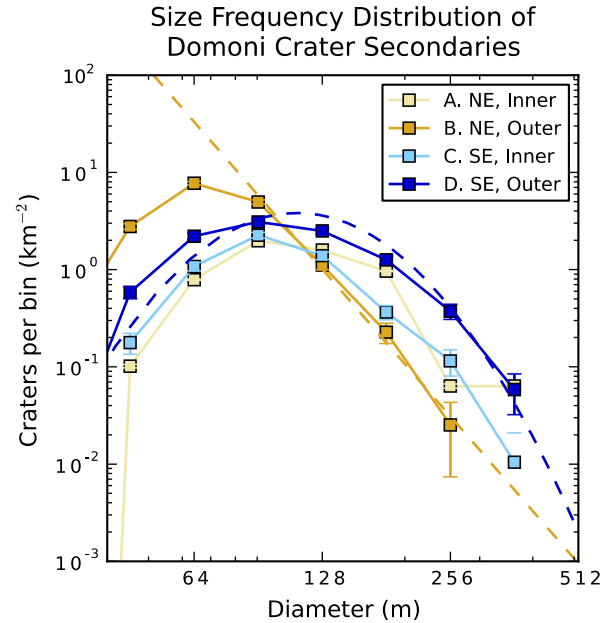


Fig. 7. Size–frequency distributions from 4 regions of Domoni secondary craters. The innermost regions from the northeast and southeast tracks in Fig. 6 are shown in light yellow and light blue, respectively, and are relatively similar. The outermost part of the northeast track with non-expanded secondaries is shown in dark yellow, and the outermost part of the southeast track with expanded secondaries is shown in dark blue. Dashed lines show the best-fit equation for the two outer regions from Table 4. Note the shift towards larger diameters between these outermost regions. (For interpretation of the references to color in this figure legend, the reader is referred to the web version of this article.)

Table 4
Parameters from best-fit power laws for Domoni size frequency distributions.

| Location | Cutoff diameter (m) | Equation |
|--------------|---------------------|---|
| A. NE, inner | 128 | $N_{\text{inc}} = 6 \times 10^7 * D_{\text{meters}}^{-3.572}$ |
| B. NE, outer | 90 | $N_{\text{inc}} = 4 \times 10^{10} * D_{\text{meters}}^{-5.027}$ |
| C. SE, inner | 128 | $N_{\text{inc}} = 7 \times 10^9 * D_{\text{meters}}^{-4.567}$ |
| D. SE, outer | 128 | $\text{Log}(N_{\text{inc}}) = -7.515 * \text{log}(D)^2 + 30.784 * \text{log}(D) - 30.944$ |

We assume that the original size distribution of secondary craters before expansion was comparable to the existing distribution of non-expanded secondaries in the outer region, and that expansion has a similar effect on craters with similar initial diameters (although it may vary for different initial diameters). This assumption is necessary to estimate the original sizes of the expanded secondaries, and we consider this an appropriate initial approximation since the regions of interest in this comparison are at the same distance from the primary crater and the slopes of their respective size–frequency distributions are similar (Table 4). However, it is important to note that the SFD for different secondary crater rays associated with a single impact, even at comparable distances from their primary crater, can vary greatly (Arvidson et al., 1976; Preblich et al., 2007), and we may be sampling regions with different crater densities. Therefore, this comparison only gives a crude estimate of secondary crater expansion. This analysis is further limited by the small number of regions that we compare, but future work will explore these initial observations in more detail.

In order to compare the size–frequency distributions of the two outermost regions, we used the equations in Table 4, solving for the crater diameters over a range of $N_{\text{incremental}}$ values. Assuming that, for any given $N_{\text{incremental}}$, the initial and final diameters can be calculated using the equations fit to the non-expanded

northeastern region and the expanded southeastern region, respectively, we can estimate the diameter change associated with expansion and determine the percent diameter change. Fig. 8 shows the result of this method, demonstrating that the degree of expansion is non-uniformly dependent on diameter, reaching a maximum for craters with an initial diameter of ~ 150 m. If there were no diameter dependence and every crater expanded by the same linear distance, we would expect the results shown in the dotted line in Fig. 8, and if every crater expanded by some fraction of its initial diameter these results would be a straight horizontal line. However, our results suggest that less expansion relative to the initial diameter is taking place in both smaller and larger craters. It is unclear why smaller craters appear to experience less expansion, but this may be an observational effect: if smaller craters underwent extensive expansion and modification, then they would be difficult or impossible to recognize in the landscape today, or could be recognizable as craters but lack a distinctive expanded morphology. In this case, our identification of craters as “non-expanded” is conservative and underestimates the importance of this process. Alternatively, we may in fact expect to see a peak like this in the degree of expansion if the larger craters have penetrated all the way through an icy layer. In that case, the amount of subsurface ice exposed and susceptible to sublimation would be limited to a certain thickness of ice exposed only at the walls of the craters, and would result in a smaller fractional diameter change associated with expansion. Moreover, the amount of expansion required to create a stabilizing lag of a given thickness is proportionally less in a larger crater. Smaller craters, which penetrate into but not through an icy layer, would expose ice on both their walls and floors, and would experience more sublimation relative to their size. The smallest craters would be expected to expand significantly, but expansion in small craters might be cut off if a sufficiently thick surface lag develops. This could more effectively coat the walls of small craters with regolith. The measured peak in initial diameter (~ 150 m) corresponds to an excavation depth of ~ 15 m (Melosh, 1989). Therefore, we suggest that the

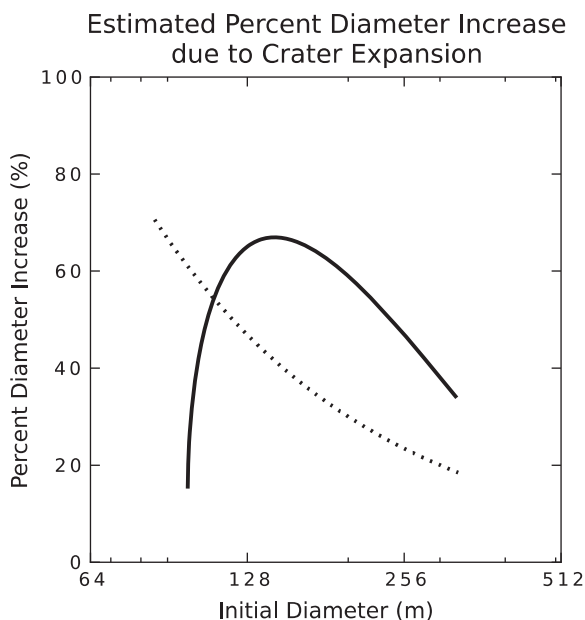


Fig. 8. The estimated percent diameter change associated with the expansion of secondary craters, calculated by comparing the best-fit equations of the SFDs for regions B and D (Fig. 7, Table 4). There is a maximum peak in expansion (relative to the initial crater diameter) at an initial diameter of 150 m. The dotted line, for reference, demonstrates what we would expect to see if craters were to expand by a fixed diameter (in this case, 60 m). See also discussion in text.

subsurface ice layer that produced the expanded secondaries within the southeastern track was at depths generally shallower than ~ 15 m. This is comparable to the depths of scalloped depressions interpreted as thermokarst landforms in both the southern hemisphere (Zanetti et al., 2010) and Utopia Planitia (Morgenstern et al., 2007), which are found to be up to tens of meters deep.

6. Parameters of expanded secondary craters

Seven HiRISE DTMs were used for detailed mapping of individual expanded secondary craters. Expanded craters were approximated as ellipses, and planar parameters (major and minor axis diameters, major axis azimuth) of each were collected using ArcGIS. Three-dimensional parameters such as depth, volume, and surface area were measured using several tools in ArcMap’s 3D Analyst toolkit. Since the expanded secondary craters that were studied here no longer have any recognizable rim or ejecta, a pre-impact surface was interpolated based on the topography just outside the perimeter of each expanded crater. Depths were calculated by subtracting the elevation of the crater’s center from the average elevation around the crater edge, and volumes were measured by subtracting the DTM surface from the interpolation of the pre-impact surface. Crater wall slopes were also measured along lines in a range of orientations from the crater center to rim using the Arcmap 3D Analyst tools to interpolate the minimum, maximum, and average slope from the DTM surface.

More than 400 expanded craters were measured from seven HiRISE DTMs within the study region (Table 2). The DTMs were spread spatially throughout the study area (Fig. 4), although many were concentrated near $\sim 50^\circ\text{N}$, and they contained a range of expanded morphologies, from very expanded and degraded to smaller and more symmetric (Fig. 9a–c). We only measure a sampling of expanded secondary craters in most of these DTMs, avoiding ones which overlapped neighboring expanded craters since, in such cases, it was not possible to produce a reasonable interpolation of the pre-impact surface. Assuming that we measured a representative sample of expanded secondary craters, we extrapolate our findings over the entire area of each DTM as well as across the entire Arcadia Planitia study area.

We suggest that the volumes of expanded craters are, to first order, a lower bound on the volume of ice that must have been sublimated from each crater. This is a reasonable first approximation because most of the material excavated during crater formation remains as continuous ejecta, thus there is no significant volume change (apart from possible density changes due to compaction or expansion). Since any raised rim and ejecta that was once present around expanded craters has since collapsed into the crater itself during expansion, the volume difference should roughly correspond to the amount of ice sublimated, although the volume of ice lost could be larger if the craters have been partially infilled by aeolian deposits. We tested this assumption by measuring both the crater bowl and rim volumes, relative to an interpolated pre-impact surface, of several non-expanded Zunil crater secondaries with well-preserved rims that were identified in HiRISE DTM DTEEC_004375_1815_003874_1815. The secondary crater volumes ranged from ~ 1 –4 times the volume of their respective rims (with a mean and median of ~ 2), suggesting that this hypothesis is at least correct to within a factor of 2.

Not surprisingly, length parameters (i.e., depth and major and minor axis diameters) were positively correlated with each other and with crater volume (Fig. 10). Expanded craters also tend to be somewhat elliptical, with eccentricities ranging from ~ 0.17 to 0.82 (median ~ 0.56), although there does not appear to be a strong correlation with latitude, which suggests that the expanded crater

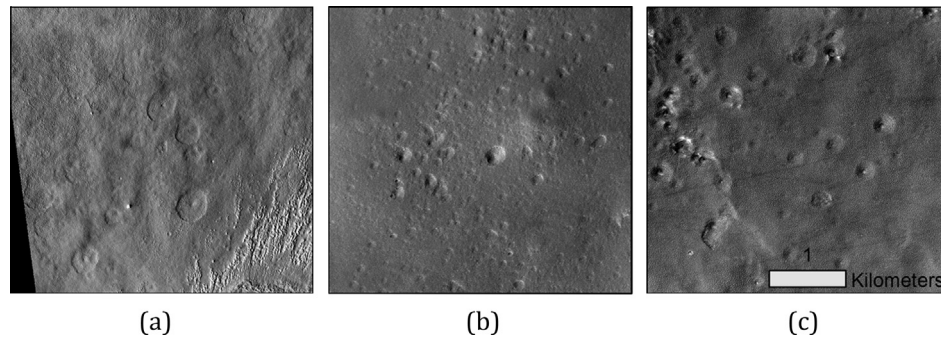


Fig. 9. Examples of expanded secondary crater morphologies spanning the latitude range of the analyzed DTMs. (a) 38°N, 192°E, from DTM c; (b) 49.5°N, 231°E, from DTM f, and (c) 57°N, 231°E, from DTM e.

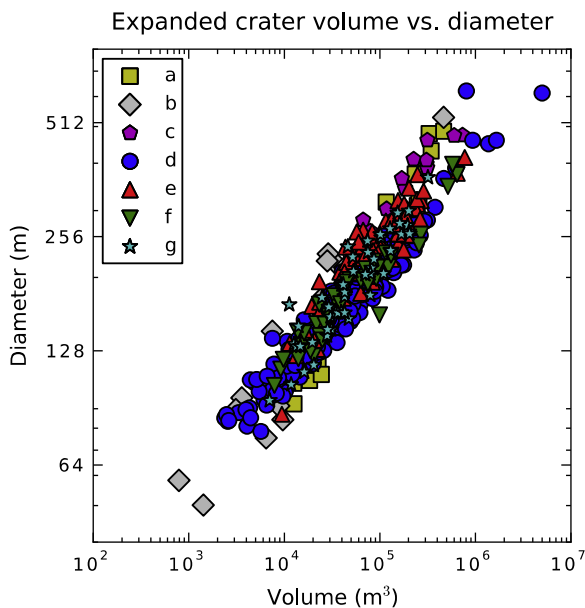


Fig. 10. The relationship between expanded crater volume and rim diameter. As expected, these parameters show a positive correlation. Letters correspond to the DTM designations in Fig. 4 and Table 2.

shape may be more highly influenced by the angle of impact or regional winds rather than any latitude-dependent expansion direction. If sublimation is the dominant control on expansion, parameters such as eccentricity and azimuth may be expected to vary with solar insolation angles and intensities, and therefore with latitude; however, since most of the DTMs analyzed are located at similar latitudes ($\sim 50^\circ\text{N}$), we are not confident that we can detect such latitudinal variations. Also, with the exception of DTM c (Table 2), where the azimuth direction of the major axis for most of the secondaries measured were between 0° and 45° east of due north, the expanded secondary craters within each individual DTM studied do not appear to have a strong azimuthal preference; this may be due to local topography effects on crater expansion or local variations in ice table properties. Furthermore, expansion may be affected by wind direction and the preferential removal or deposition of wind-blown material inside these craters.

6.1. Crater volumes

The total volume lost from all the measured expanded craters in each DTM ranged from $\sim 1 \times 10^6 \text{ m}^3$ (from 24 craters in DTM b in Table 2) to $\sim 2.1 \times 10^7 \text{ m}^3$ (from 197 craters in DTM d in Table 2). When divided across the total planar area of the expanded craters

measured within each DTM, we find that this volume translates into an average thickness of $\sim 1.9\text{--}4.7 \text{ m}$. These are lower limits on the thicknesses due to the possibility for aeolian infill subsequent to crater expansion and because it assumes uniform sublimation throughout the whole crater, although it is more likely that sublimation was not entirely symmetric along all aspects of the crater.

6.2. Crater depths

Expanded crater depths may be related to the depth to or thickness of the subsurface ice layer involved in their thermokarstic expansion. The expanded craters that we measured tend to have depths between ~ 2 and 20 m , although there are a few shallower and deeper craters in a small number of the DTMs analyzed. Crater depth increases nearly linearly with diameter over the range of expanded craters measured, roughly following the equation: $D = 12.4 * d + 105$. Most of the DTMs had a median crater depth around 5.7 m , although one of them, DTM b (Table 2), contains expanded craters that appear consistently shallower than that of the other DTMs (median $\sim 3.15 \text{ m}$). This location also represents a morphological exception to the observed pattern where expansion appears more concentrated overlying older ejecta; although this DTM contains a small, 1-km crater, it appears that the smaller secondary craters overlying the ejecta of this crater have undergone little to no expansion, whereas expanded craters are seen around and at the fringes of the ejecta (Fig. 11). This dichotomy in expansion morphologies may be due to the presence of relatively deeper regolith above subsurface ice in this location, so not all of the overlying secondary craters penetrated deeply enough to expose and sublimate ice. At the steeper edge of the ejecta, less overlying regolith may be present, allowing these craters to expose ice and undergo expansion.

When crater depths are averaged over binned diameters to minimize the effects of location and crater size, we find that depths increase steadily with increasing diameter until $\sim 10 \text{ m}$, at which point the depths start to level off, with averages around $10\text{--}12 \text{ m}$ (Fig. 12). There are a few exceptions at larger diameters, but those bins also contain fewer craters and have larger errors. Note that this leveling off of expanded crater depths occurs near the maximum depth of the ice layer that was estimated from the comparisons of expanded and non-expanded secondary craters in the vicinity of Domoni crater ($\sim 15 \text{ m}$). This may further suggest that a widespread ice layer at around this depth or thickness is present throughout Arcadia Planitia in the areas where expanded secondary craters are found; however, the precise relationship between the depth or thickness of the icy layer and the expanded morphology is presently unclear, and it is alternatively possible that the larger craters more effectively trap atmospheric dust and ice, and are more easily infilled.

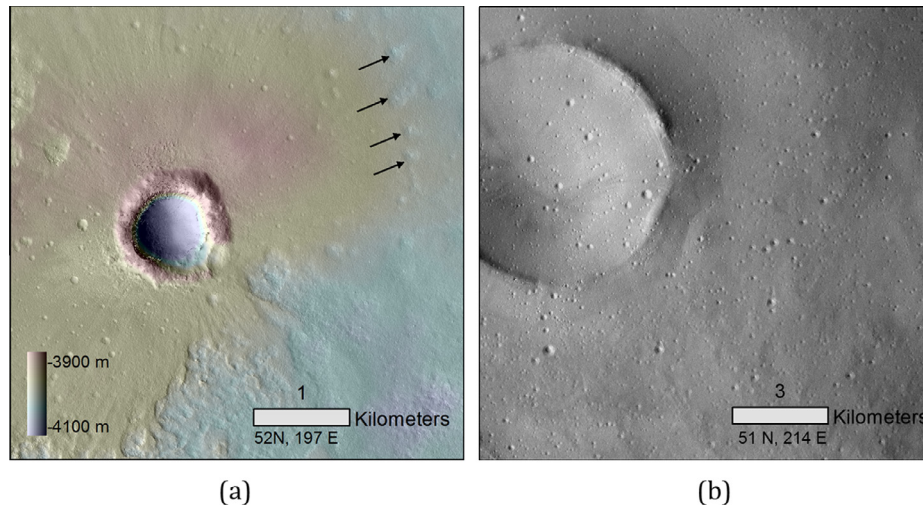


Fig. 11. Expanded secondary craters in (a) HiRISE DTM 027027_2325_027370_2325_A01 (52N, 197E), compared to those in (b) CTX image B20_017506_2325_XN_52N147W (51.5N, 214E). Note that expanded craters in (a) are concentrated near the edges of the small primary crater's ejecta, whereas expanded craters cover both the infill and the surrounding ejecta of the larger primary crater in (b).

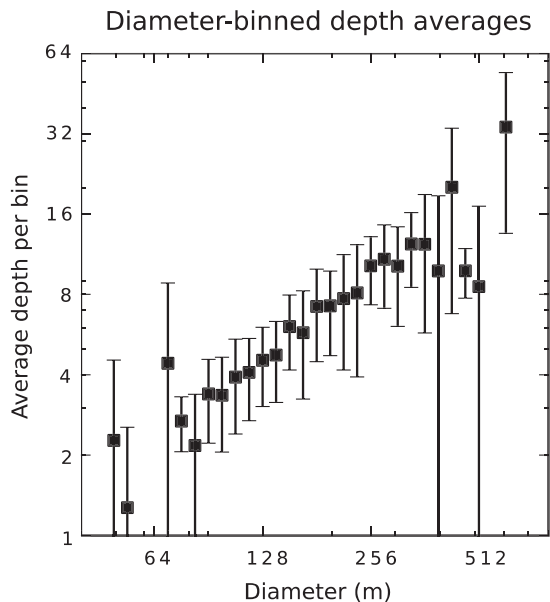


Fig. 12. The average expanded crater depth split into diameter bins at intervals of $2^{1/8}D$. With the exception of very small and very large diameters, each bin contained more than 30 craters. Error bars are one standard deviation.

6.3. Depth/Diameter ratios

Crater depth-to-diameter (d/D) ratios are a common measure used when comparing impact craters. It is widely accepted that the d/D ratio for small, fresh, simple craters is typically around 0.2 (Pike, 1980), although secondary craters tend to have lower d/D ratios. Pike and Wilhelms (1978) found that secondary craters on the Moon have d/D ratios around 0.11, and McEwen et al. (2005) observed a typical d/D ratio of ~ 0.08 for craters interpreted to be secondaries on Mars. We calculated d/D ratios for the expanded craters using both the major and minor axis diameters, and consistently found that the ratios were lower than the previously-observed values for secondary craters. This is expected since the expansion process increases the crater diameter and, due to infilling, also makes the crater shallower. It would therefore seem

reasonable that the lower the d/D ratio for an expanded crater, the more it has been expanded/degraded over time.

We identified the average and range of d/D values that were measured within each DTM analyzed, as well as the average d/D ratios for binned diameters across all DTMs to correct for any effects of latitude or diameter range. The individual averages for each DTM are shown in Fig. 13a, and the diameter-binned average d/D ratios are shown in Fig. 13b. DTM c (Table 2) is the lowest-latitude DTM in this study; it also has the lowest range of d/D values and appears to have been the most degraded (Fig. 9a). However, when averaged over all DTMs, the average d/D ratio for nearly all diameter bins collapses to ~ 0.035 (Fig. 13b). This may be due to sublimation effects that are proportional to diameter or more rapid infilling of larger craters.

6.4. Crater wall slopes

Wall slopes for each crater were measured in six orientations: due north and due south, and along both the north- and south-facing radii of the major and minor axes (since each expanded crater was approximated as an ellipse). Slight asymmetries between north- and south-facing slopes were observed in some of the DTMs analyzed. However, many of the DTMs did not show a strong directional preference, nor were there apparent trends with latitude. This may be because crater expansion takes place over climatic changes that can have an averaging effect or because creep can become the dominant force over time. It is notable that the slopes of expanded crater walls are not as asymmetric as scalloped depressions, another feature commonly associated with sublimation processes and similarly observed in the mid latitudes (40–50°N, Morgenstern et al., 2007). We consider it possible that, given more time, expanded secondary craters could develop stronger slope asymmetries and evolve into scalloped depressions. Alternatively, scallops might become more symmetric if lag development halts sublimation on the warm surface while creep continues to reduce the slope of the colder slopes.

6.5. Preservation of ice beneath ejecta: A DTM case study

One of the DTMs studied, letter d in Table 2, is particularly interesting because it straddles the edge of the inner and outer ejecta layers of an older primary DLE crater ($D = 15$ km), and there

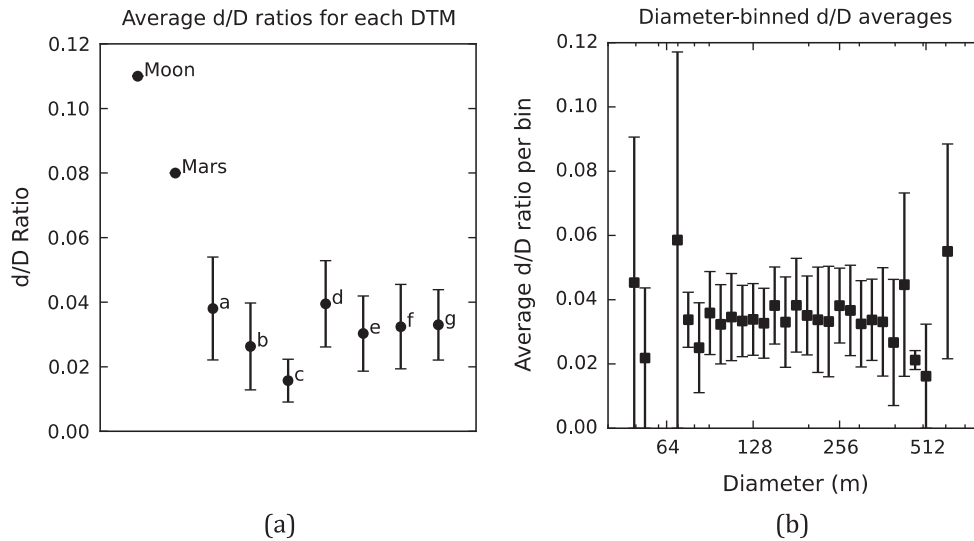


Fig. 13. Average d/D ratios for each DTM, ± 1 standard deviation, compared to typical secondary crater values on the Moon and Mars (a) (letters correspond to DTM designations in Fig. 4 and Table 2), and the d/D ratio from all DTMs averaged over diameter bins at intervals of $2^{1/8}D$ to remove possible latitudinal influence, where error bars are one standard deviation (b).

are distinct morphological differences between the expanded secondary craters within the two topographic regions (Fig. 14). Another transition to craters that do not appear expanded occurs at the edge of the outer ejecta and the surrounding terrain (see HiRISE image ESP_018007_2305). Since these secondary craters are all found in close association, it is likely that they all resulted from the same impact event, and thus have had an identical amount of time to undergo expansion. If the surface and subsurface properties throughout this DTM were effectively identical, then we would expect that thermokarstic expansion would alter all secondary craters of a given size in similar ways. However, as Fig. 14 demonstrates, the secondary craters in the northern part of the DTM, overlying the inner ejecta, appear to be more expanded than those in the southern part of the DTM, which overlies the outer ejecta. Therefore, we hypothesize that this dichotomy is the result of different subsurface volatile abundances within the two layers of crater ejecta. An alternative explanation for this dichotomy is that the two populations sample different regions of a secondary crater ray with different initial size distributions, but the association of the transition with the layered ejecta boundary makes it difficult to rule out the effect of variations in surface properties. Differences in regolith properties within the two ejecta layers may also play a role if the inner layer is better suited for ice lens growth.

Measurements of the expanded craters within the DTM confirm this dichotomy. A comparison of the size–frequency distributions of the expanded craters within the two regions reveals that there are more large-diameter craters and a shallower SFD slope in the northern section of the DTM (Fig. 15), likely due to the greater degree of expansion observed. There were a total of 134 craters measured in the elevated, northern region, which had an areal extent of ~ 42 km², and 54 measured in the southern region (area ~ 21 km²), while 11 expanded craters were found on or close to the elevation dichotomy and were not included in the SFD. We also calculated the thickness of ice lost in both the northern and southern regions as per Section 6.1, above, and found a very clear difference. A total volume of 1.8×10^7 m³ (1.4×10^5 m³/crater) was lost from the craters measured in the northern region, whereas only $\sim 1 \times 10^6$ m³ (1.9×10^4 m³/crater) was lost from those in the southern region, corresponding to approximate average thicknesses of ice lost of 2.93 and 1.48 m, respectively. This may suggest that more ice was initially present beneath the

older crater's ejecta or that there was a thinner covering lag, allowing for more extensive expansion.

7. Discussion

We find that there are an estimated $>10^6$ secondary craters with diameters greater than ~ 50 m within our study area in and around Arcadia Planitia, mostly associated with four primary impact craters (Domoni, Steinheim, Gan, and an unnamed 6-km crater) ranging from 6 to 19 km in diameter and 18–70 Myr in age. This estimate is roughly consistent with previous studies of Zunil crater on Mars, a 10-km impact crater in Elysium Planitia (166.19°E, 7.7°N), which was found to have $>10^7$ secondary craters >15 m in diameter and $\sim 10^5$ secondary craters greater than 50 m in diameter (McEwen et al., 2005; Preblich et al., 2007). However, a unique feature of many of the Arcadia Planitia secondary craters is that they show evidence for thermokarstic expansion, which suggests that there must have been extensive excess ice throughout the area at the time of their formation. These expanded secondary craters have been linked to at least the four source impact craters described above. Recent orbital measurements show a present abundance of excess ice in Arcadia Planitia (e.g. Boynton et al., 2002; Bramson et al., 2013) and little terrain dissection due to ice loss is observed compared to comparable latitudes around the planet (Mustard et al., 2001). Broad-scale loss of subsurface ice through sublimation-induced terrain dissection would have resulted in the destruction of the expanded craters (Dundas et al., 2014b, submitted for publication); since these morphologies remain preserved, we argue that the ice in Arcadia Planitia antedates the formation of the source primary impact craters, and is at least tens of millions of years old.

Orbital instruments such as the Gamma Ray Spectrometer and radar detectors (SHARAD and MARSIS) have previously detected subsurface ice on different vertical scales (<1 m and tens to hundreds of meters, respectively). However, there is an intermediate depth range that remains inaccessible to these direct means of measurement. The study of expanded secondary craters allows us to probe that depth indirectly; typical depths of expanded craters in Arcadia Planitia lie in this intermediate range, up to about 15 m. Since the formation mechanism for expanded craters involves the thermokarstic loss of excess ice, we use these features

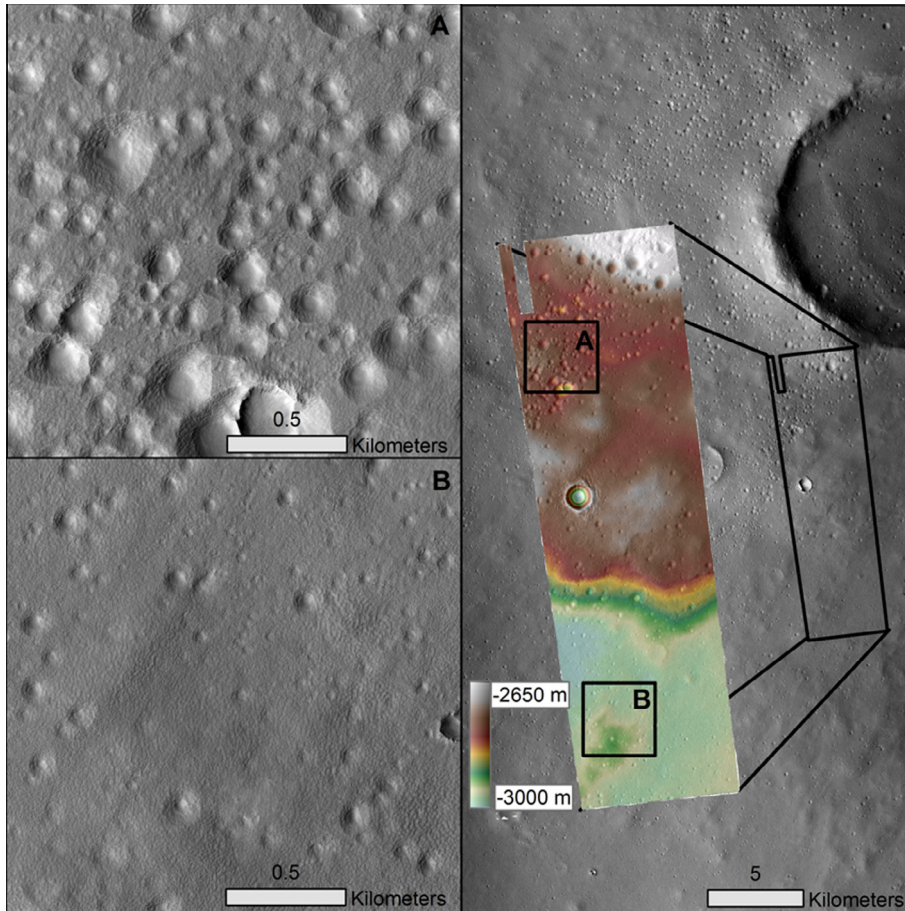


Fig. 14. DTM d (Table 2) in context (right), showing the elevation dichotomy where the DTM overlies the ejecta boundary of an older crater (right). Insets at left show expanded craters from the ejecta (A) and the surrounding terrain (B) at the same scale, for comparison.

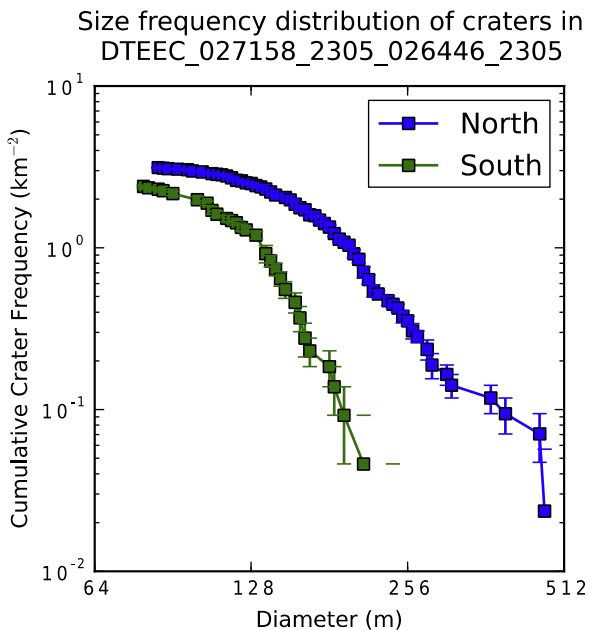


Fig. 15. The size frequency distributions of expanded crater populations in the northern and southern region of DTM d. Note the shift towards larger diameters for expanded craters in the northern section overlying the ejecta of an older crater.

to infer the presence of an excess ice layer of uncertain thickness within the uppermost 20 m of the surface in the region of Arcadia Planitia.

By extrapolating the measured estimates of ice lost from the expanded craters measured in the HiRISE DTMs (with approximate average ice thicknesses ranging from 1.86 to 4.74 m) across the entire study region using the total area of expanded craters that were measured by the CTX mapping ($7.5 \times 10^{10} \text{ m}^2$), we estimate that the total ice lost from sublimation during the formation of all the mapped expanded craters in Arcadia Planitia was $\sim 140\text{--}360 \text{ km}^3$, equivalent to a global layer of 1–2.5 mm. This is at least 100 times more water than the 10 μm present in the martian atmosphere today, and if all the water vapor released by the sublimation expansion of the Arcadia Planitia secondary craters were to have been re-deposited on the north polar layered deposits, it would have produced a layer $\sim 17\text{--}45 \text{ cm}$ thick, although spread over at least four events. It is challenging to estimate the total volume of ice remaining in Arcadia Planitia because the distribution of expanded secondary craters is heterogeneous due to the combined effects of the original distribution of the secondary craters formed by the primary impacts of interest and heterogeneities in the distribution of subsurface ice in the region. However, it seems likely that there is still extensive ice present to this day: even if only 20% of the study region retains a 10-m thick layer of excess subsurface ice, an ice volume greater than 6000 km^3 is currently buried in the Arcadia Planitia, equivalent to a global ice layer $>4.1 \text{ cm}$ thick.

It has been suggested that impacts can liberate subsurface water and cause widespread environmental effects (Segura et al., 2002; Colaprete et al., 2004) which may have played a strong role in the climate of early Mars, during the late heavy bombardment period and when most of the martian valley networks are thought to have formed. Secondary craters can also liberate large amounts of near-surface ice in excess of the amount of water liberated by

their associated primary impact (Zahnle and Colaprete, 2007), which could remain relevant on Mars during the present epoch. Indeed, the release of 140–360 km³ of water vapor into the martian atmosphere, as estimated to have been produced in the formation of the Arcadia Planitia expanded secondary craters, would have affected atmospheric conditions during the time periods over which they formed. The timescale for crater expansion itself, based on thermal and landscape evolution models, is at least tens to hundreds of thousands of years (Dundas et al., 2014b), suggesting that the release of water vapor from these expanding secondary craters would have taken place gradually, but the effect would have been strongest immediately after impact when sublimation was most rapid.

The secondary craters closest to each primary impact do not appear to have undergone much or any expansion as compared to the more distant secondaries, although it is not entirely clear why this would be the case. It is possible that the region was so highly disturbed at the time of the impact that most of the ice present then may have been vaporized, or that it is a function of the lower impact velocities expected for nearby secondary craters. Alternatively, these secondary craters may have undergone so much expansion over time that the central bowl-shaped region common in expanded craters was not preserved in these regions, or debris surges from interacting ejecta could have covered exposed ice and precluded sublimation. It should be noted that, at HiRISE resolution, some secondary craters close to Crater α did appear to have undergone slight expansion, which suggests that CTX resolution may not always be sufficient to detect the expanded morphologies.

Mapping expanded secondary craters also revealed that a disproportionate fraction of the preserved secondary craters in Arcadia Planitia are localized within or on the ejecta of older primary impact craters, some of which have been identified as perched or pedestal craters. This is consistent with the idea that these types of craters may have preserved ice beneath their ejecta, which could have been exposed at a later time when the overlying secondary craters were formed and subsequently expanded. This would also suggest that the ice, at least in some locations, is even older than our minimum estimate of tens of millions of years old; Kadish and Head (2014) use superposed craters to constrain the ages of pedestal craters and argue that widespread ice deposits have likely recurred frequently over the past 250 Myr, although few of their dated pedestal craters appear to coincide with our study area. However, there is some uncertainty in regards to the presence of expanded secondary craters within the bowls of older impact craters, since ice within the craters cannot have had the same protective ejecta cover and must have been deposited afterwards. It is possible that later events of ice deposition may have either coincided with or been the primary cause of post-impact infilling of these older craters, which could account for the presence of post-dated secondary crater expansion. Additional observations of the expanded crater populations in this region, focused on those that coincide with older ejecta, may offer further insights about multiple episodes of ice deposition.

The orbital evolution of Mars implies that the planet's climate should have undergone significant fluctuations even in relatively recent history, and that the stability of ground ice should have similarly varied across the planet. Models have shown that the obliquity of Mars has fluctuated greatly over the past 20 million years (Laskar et al., 2004), and that the distribution of insolation and the regions and depths at which ice is stable have varied accordingly (Mellon and Jakosky, 1995; Chamberlain and Boynton, 2007). Several hypotheses have been proposed in regards to the climate and obliquity conditions, as well as ice source locations, associated with the formation of the mid-latitude ice sheet. These include the transport of polar ice to the mid latitudes during

periods of high obliquity (Jakosky and Carr, 1985; Head et al., 2003) and the transport of equatorial ice during periods of moderate (25–35°) (Madeleine et al., 2009) or low obliquity (<25°) (Levrard et al., 2004). Regardless, it is largely thought that, given the relatively short-period fluctuations in orbital parameters, mid-latitude ice should not be stable for longer than a few hundreds of thousands of years, especially not in the uppermost meters of the regolith. It has been argued that the ice found in the martian mid latitudes formed during a geologically-recent ice age, ~2.1–0.5 Myr ago, and that it must be retreating due to its current instability (Head et al., 2003). This work, on the other hand, suggests that the ice in Arcadia Planitia is in fact much older, on the order of tens of millions of years old (perhaps >70 Myr, based on the estimated age of the oldest primary crater to have been a source for expanded secondary craters, but we caution that the crater age estimates are imprecise), and it is unclear how the subsurface ice layer could remain intact over such long time scales. However, Schorghofer and Forget (2012) have modeled the evolution of an ice sheet to explore the presence of shallow excess ice in the mid to high latitudes on Mars, and suggest that a lag deposit should form rapidly over an ice sheet if a small fraction of dust was intermixed with the ice at the time of deposition. This mechanism could have allowed for the rapid burial of an ancient ice layer emplaced in Arcadia Planitia, preserving thick, excess ice at some depth over long timescales. Schorghofer and Forget (2012) also argued that the best explanation for the presence of lower-latitude (<43°N) ice-exposing impact craters is a recently-deposited ice sheet that has not reached equilibrium with the atmosphere. Some of these low-latitude, icy impacts are located in Arcadia Planitia, so our results are incongruous with such a young ice sheet if they are exposing the same ice layer into which the expanded secondary craters impacted. However, we cannot rule out the possibility of later depositions of ice after the formation of the secondary craters we discuss here, as long as any subsequent deposition did not infill and erase the expanded craters.

A candidate explanation for this excess ice layer is surface deposition in the form of ice or snow, which was subsequently buried and compressed. This formation mechanism would have required widespread snowfall tens of millions of years ago, which could have been buried by the development of a lag deposit, as discussed above, and was preserved in the subsurface to this day. Another mechanism for the formation of excess ice is the initiation and growth of ice lenses, which can build up a thick layer of ice over many seasonal cycles depending on climatic and soil properties (Sizemore et al., in press). This process is thought to be commonplace during the Amazonian period, and likely produced some degree of excess subsurface ice in Arcadia Planitia even after the formation of the expanded secondary craters that we observe today. However, the timescales and depths that this mechanism affects suggest that it cannot solely account for the deeper ice sheet in Arcadia Planitia; some models indicate that ice lens initiation and growth only occurs within the uppermost tens of centimeters of regolith, and that it takes on the order of tens of thousands of years to develop centimeters to decimeters of excess ice (Sizemore et al., in press).

Based on our observations, and on the previous discussion, we propose that a massive ice sheet, perhaps the result of snowfall, was deposited in Arcadia Planitia >20 million years ago and that it was preserved beneath a lag deposit that likely developed fairly quickly. Much of the ice was gradually lost, except in special circumstances such as below impact ejecta. The secondary impact craters that we observe in this study formed concurrently with their primary craters, locally exposing this massive ice sheet and undergoing expansion over tens to hundreds of thousands of years. Significant loss of the remnants of this ancient, massive ice sheet could not have occurred, since a widespread deflation of the sur-

face would have also destroyed the expanded morphologies that we observe today. However, our study does not necessarily preclude the later formation of near-surface excess ice in the uppermost centimeters to decimeters due to ice lens formation or more recent snowfall, which may account for the ice that has been observed in the uppermost meter of the martian surface.

8. Conclusions

Extensive regions of expanded secondary craters are found in Arcadia Planitia and correlate well with regions where shallow (<1 m) excess ice has been detected by orbital measurements, although some heterogeneity is observed. The leading hypothesis for crater expansion is thermokarstic ice loss via sublimation following an impact into excess ice. The preservation of expanded craters over time suggests that the excess ice layer must pre-date the formation of the craters without significant loss in the terrain surrounding these features, indicating that this ice is still present throughout the subsurface of Arcadia Planitia. The secondary craters in this region appear to be largely sourced from 4 primary craters ranging from 6 to 20 km in diameter and 18–70 million years in age. Since these secondary craters formed at the same time as their source primary and remain preserved to this date, we can constrain the age of the subsurface ice layer associated with their formation to a minimum of tens of millions of years old. It is notable that expanded craters are more abundant overlying older craters, including perched and pedestal craters, providing further evidence that these features preferentially preserve ice.

The persistence of ice over such long timescales is unexpected, since climate and ice stability models indicate that obliquity cycles should lead to periodic loss and accumulation of ice in the mid latitudes on timescales much shorter than the lifetime that we find here. It is possible that Arcadia Planitia is unique in its preservation of ancient ice – secondary crater fields appear uncommon in other mid-latitude terrains, which also seem to have undergone more extensive dissection attributed to ice loss, indicating more recent sublimation-associated resurfacing. Surface properties likely contribute to preserving ice in this region; since Arcadia Planitia has a high albedo and more dust cover than other mid-latitude terrains, we would expect the shallow subsurface to be colder and that ice should therefore be more stable. Utopia Planitia has also been noted for its abundance of excess ice due to the presence of scalloped terrain and subsurface reflections in SHARAD (Stuurman et al., 2014), but has lower albedo and therefore ice may be less stable or younger in that region of the northern plains.

Large quantities of ice were likely liberated during the expansion of these secondary craters. We estimate that the minimum volume of ice sublimated during the expansion of the Arcadia Planitia expanded secondaries is approximately 140–360 km³. This water vapor would have been released to the atmosphere slowly over time, but may have had a temporary impact on the martian climate. A conservative estimate suggests that the amount of ice remaining in the subsurface of Arcadia Planitia is >6000 km³, equivalent to a global ice layer >4.1 cm thick. Much of this is likely buried below dry regolith and does not interact with the atmosphere, but could be a water resource for future human exploration of Mars.

Acknowledgments

We thank Sarah Mattson and student workers at the University of Arizona for the production of HiRISE Digital Terrain Models. Hanna Sizemore and Mikhail Kreslavsky provided detailed, constructive reviews. Funding for this research was provided by the Mars Reconnaissance Orbiter project.

References

- Arvidson, R., Drozd, R., Guinness, E., Hohenberg, C., Morgan, C., 1976. Cosmic ray exposure ages of Apollo 17 samples and the age of Tycho. In: *Proceedings of the Lunar Science and Conference*, vol. 7, pp. 2817–2832.
- Bandfield, J.L., Feldman, W.C., 2008. Martian high latitude permafrost depth and surface cover thermal inertia distributions. *J. Geophys. Res.* 113, E08001.
- Barlow, N.G., 2005. A review of martian impact crater ejecta structures and their implications for target properties. *Geol. Soc. Am. Spec. Pap.* 384, 433–442.
- Barlow, N.G., Bradley, T.L., 1990. Martian impact craters: Correlations of ejecta and interior morphologies with diameter, latitude, and terrain. *Icarus* 87, 156–179.
- Barrett, A., Balme, M., Patel, M., Hagerman, A., 2013. The latitudinal distribution of putative periglacial sites on the northern martian plains. *EGU Gen. Assem.*, 10.
- Boyce, J.M., Mouginis-Mark, P.J., 2006. Martian craters viewed by the thermal emission imaging system instrument: Double-layered ejecta craters. *J. Geophys. Res.* 111, E10005.
- Boynton, W.V. et al., 2002. Distribution of hydrogen in the near surface of Mars: Evidence for subsurface ice deposits. *Science* 297 (81), 81–85.
- Bramson, A.M., Byrne, S., Putzig, N.E., Plaut, J.J., Mattson, S., Holt, J.W., 2013. Thick subsurface water ice in Arcadia Planitia, Mars. *Am. Geophys. Union, Fall Meet.*, Abstract #P43D-05.
- Byrne, S. et al., 2009. Distribution of mid-latitude ground ice on Mars from new impact craters. *Science* 325, 1674–1676.
- Carr, M.H., 1996. *Water on Mars*. Oxford Univ. Press, p. 229.
- Chamberlain, M.A., Boynton, W.V., 2007. Response of martian ground ice to orbit-induced climate change. *J. Geophys. Res.* Planets 112, E06009.
- Colaprete, A., Haberle, R.M., Segura, T.L., Toon, O.B., Zahnle, K., 2004. The effects of impacts on the early martian climate. In: *Second Conference on Early Mars*.
- Dundas, C.M., Byrne, S., 2010. Modeling sublimation of ice exposed by new impacts in the martian mid-latitudes. *Icarus* 206, 716–728.
- Dundas, C.M. et al., 2014a. HiRISE observations of new impact craters exposing martian ground ice. *J. Geophys. Res.* – Planets 119, 109–127.
- Dundas, C.M., Byrne, S., McEwen, A.S., 2014b. Clean ground ice on Mars: Evidence from spacecraft, fresh craters, and thermokarst. In: *8th International Conference on Mars*, Abstract #1375.
- Dundas, C.M., Byrne, S., McEwen, A.S., submitted for publication. Modeling the development of martian sublimation thermokarst landforms.
- Fastook, J.L., Head, J.W., Forget, F., Madeleine, J.-B., Marchant, D.R., 2011. Evidence for Amazonian northern mid-latitude regional glacial land systems on Mars: Glacial flow models using GCM-driven climate results and comparisons to geological observations. *Icarus* 216, 23–39.
- Feldman, W.C. et al., 2004. Global distribution of near-surface hydrogen on Mars. *J. Geophys. Res.* 109, E09006.
- Feldman, W.C. et al., 2011. Mars Odyssey neutron data: 2. Search for buried excess water ice deposits and nonpolar latitudes on Mars. *J. Geophys. Res.* 116, E11009.
- Fisher, D.A., 2005. A process to make massive ice in the martian regolith using long-term diffusion and thermal cracking. *Icarus* 179, 387–397.
- Garvin, J.B., Frawley, J.J., 1998. Geometric properties of martian impact craters: Preliminary results from the Mars orbiter laser altimeter. *Geophys. Res. Lett.* 25, 4405–4408.
- Hartmann, W.K., 2005. Martian cratering 8: Isochron refinement and the chronology of Mars. *Icarus* 174, 294–320.
- Head, J.W., Mustard, J.F., Kreslavsky, M.A., Milliken, R.E., Marchant, D.R., 2003. Recent ice ages on Mars. *Nature* 426, 797–802.
- Head, J.W. et al., 2005. Tropical to mid-latitude snow and ice accumulation, flow and glaciation on Mars. *Nature* 434, 346–351.
- Holt, J.W., et al., 2008. Radar sounding evidence for ice within lobate debris aprons near Hellas Basin, mid-southern latitudes of Mars. In: *39th Lunar and Planetary Science Conference*, p. 2441.
- Jakosky, B.M., Carr, M.H., 1985. Possible precipitation of ice at low latitudes of Mars during periods of high obliquity. *Nature* 315, 559–561.
- Kadish, S.J., Barlow, N.G., 2006. Pedestal crater distribution and implications for a new model of formation. In: *Lunar and Planetary Science Conference XXXVII*, p. 1254.
- Kadish, S.J., Head, J.W., 2011. Impacts into non-polar ice-rich paleodeposits on Mars: Excess ejecta craters, perched craters, and pedestal craters as clues to Amazonian climate history. *Icarus* 215, 34–46.
- Kadish, S.J., Head, J.W., 2014. The ages of pedestal craters on Mars: Evidence for a late-Amazonian extended period of episodic emplacement of decameters-thick mid-latitude ice deposits. *Planet. Space Sci.* 91, 91–100.
- Kadish, S.J., Barlow, N.G., Head, J.W., 2009. Latitude dependence of martian pedestal craters: Evidence for sublimation-driven formation mechanism. *J. Geophys. Res.* 114, E10001.
- Kirk, R.L. et al., 2008. Ultrahigh resolution topographic mapping of Mars with MRO HiRISE stereo images: Meter-scale slopes of candidate Phoenix landing sites. *J. Geophys. Res.* 113, E00A24. <http://dx.doi.org/10.1029/2007JE0030000>.
- Korteniemi, J., Kreslavsky, M.A., 2013. Patterned ground in the martian high northern latitudes: Morphology and age constraints. *Icarus* 225, 960–970.
- Kossacki, K.J., Portyankina, G., Thomas, N., 2011. The evolution of exposed ice in a fresh mid-latitude crater on Mars. *Icarus* 211, 195–206.
- Kostama, V.-P., Kreslavsky, M.A., Head, J.W., 2006. Recent high-latitude icy mantle in the northern plains of Mars: Characteristics and ages of emplacement. *Geophys. Res. Lett.* 33, L11201.
- Laskar, J., Correia, A.C., Gastineau, M., Joutel, F., Levrard, B., Robutel, P., 2004. Long term evolution and chaotic diffusion of the insolation quantities of Mars. *Icarus* 170, 343–364.

- Leighton, R.B., Murray, B.C., 1966. Behavior of carbon dioxide and other volatiles on Mars. *Science* 153, 136–144.
- Levrard, B., Forget, F., Montmessin, F., Laskar, J., 2004. Recent ice-rich deposits formed at high latitudes on Mars by sublimation of unstable equatorial ice during low obliquity. *Nature* 431, 1072–1075.
- Levy, J.S., Marchant, D.R., Head, J.W., 2010. Thermal contraction crack polygons on Mars: A synthesis from HiRISE, Phoenix, and terrestrial analog studies. *Icarus* 206, 229–252.
- Madeleine, J.B., Forget, F., Head, J.W., Levrard, B., Montmessin, F., Millour, E., 2009. Amazonian northern mid-latitude glaciation on Mars: A proposed climate scenario. *Icarus* 203, 390–405.
- Malin, M.C. et al., 2007. Context camera investigation on board the Mars Reconnaissance Orbiter. *J. Geophys. Res.* 112, E05S04.
- McEwen, A.S., Bierhaus, E.B., 2006. The importance of secondary cratering to age constraints on planetary surfaces. *Ann. Rev. Earth Planet. Sci.* 34, 535–567.
- McEwen, A.S., Preblich, B.S., Turtle, E.P., Artemieva, N.A., Golombek, M.P., Hurst, M., et al., 2005. The rayed crater Zunil and interpretations of small impact craters on Mars. *Icarus* 176, 351–381.
- McEwen, A.S. et al., 2007. Mars Reconnaissance Orbiter's High Resolution Imaging Science Experiment (HiRISE). *J. Geophys. Res.* 112, E05S02.
- Mellon, M.T., Jakosky, B.M., 1995. The distribution and behavior of martian ground ice during past and present epochs. *J. Geophys. Res.* 100 (E6), 11781–11799.
- Mellon, M.T., Feldman, W.C., Prettyman, T.H., 2004. The presence and stability of ground ice in the southern hemisphere of Mars. *Icarus* 169, 324–340.
- Mellon, M.T., Arvidson, R.E., Marlow, J.J., Phillips, R.J., Asphaug, E., 2008. Periglacial landforms at the Phoenix landing site and the northern plains of Mars. *J. Geophys. Res.* 113, E00A23.
- Mellon, M.T. et al., 2009a. Ground ice at the Phoenix landing site: Stability state and origin. *J. Geophys. Res.* 114, E00E07.
- Mellon, M.T. et al., 2009b. The periglacial landscape at the Phoenix landing site. *J. Geophys. Res.* 114, E00E06.
- Melosh, H.J., 1989. *Impact Cratering: A Geologic Process*. Oxford University Press, New York.
- Meresse, S., Costard, F., Mangold, N., Baratoux, D., Boyce, J.M., 2006. Martian perched craters and large ejecta volume: Evidence for episodes of deflation in the northern lowlands. *Meteor. Planet. Sci.* 41, 1647–1658.
- Morgenstern, A., Hauber, E., Reiss, D., van Gasselt, S., Grosse, G., Schirmermeister, L., 2007. Deposition and degradation of a volatile-rich layer in Utopia Planitia and implications for climate history on Mars. *J. Geophys. Res.* 112, E06010.
- Mouginis-Mark, P., 1981. Ejecta emplacement and modes of formation of martian fluidized ejecta craters. *Icarus* 45, 60–76.
- Mouginis-Mark, P.J., Boyce, J.M., 2012. Tooting crater: Geology and geomorphology of the archetype large, fresh, impact crater on Mars. *Chemie der Erde* 72, 1–23.
- Mouginis-Mark, P.J., Garbeil, H., 2007. Crater geometry and ejecta thickness of the martian impact crater tooting. *Meteor. Planet. Sci.* 42, 1615–1625.
- Mouginis-Mark, P.J., Hayashi, J.N., 1993. Shallow and deep fresh impact craters in Hesperia Planum, Mars. *Earth, Moon, Planets* 61, 1–20.
- Mouginot, J., Pommerol, A., Kofman, W., Beck, P., Schmitt, B., Herique, A., et al., 2010. The 3–5 MHz global reflectivity map of Mars by MARSIS/Mars Express: Implications for the current inventory of subsurface H₂O. *Icarus* 210, 612–625.
- Mouginot, J., Pommerol, A., Beck, P., Kofman, W., Clifford, S.M., 2012. Dielectric map of the martian northern hemisphere and the nature of plain filling materials. *Geophys. Res. Lett.* 39, L02202.
- Mustard, J.F., Cooper, C.D., Rifkin, M.K., 2001. Evidence for recent climate change on Mars from the identification of youthful near-surface ground ice. *Nature* 412, 411–414.
- Nunes, D.C. et al., 2011. Shallow Radar (SHARAD), pedestal craters, and the lost martian layers: Initial assessments. *J. Geophys. Res.* 116, E04006.
- Oberbeck, V.R., Morrison, R.H., 1973. On the formation of the lunar herringbone pattern. In: *Lunar and Planetary Institute Science Conference Abstracts*, vol. 4, pp. 107–123.
- Picardi, G. et al., 2004. Performance and surface scattering models for the Mars Advanced Radar for Subsurface and Ionosphere Sounding (MARSIS). *Planet. Space Sci.* 52, 149–156.
- Pietrek, A., Wulf, G., Kenkmann, T., 2013. Detailed geologic mapping (1:80,000-scale) of Steinheim crater, Mars. In: *Lunar and Planetary Science Conference*.
- Pike, R.J., 1980. Formation of complex impact craters: Evidence from Mars and other planets. *Icarus* 43, 1–19.
- Pike, R.J., Wilhelms, D.E., 1978. Secondary impact craters on the Moon: Topographic form and geologic process. In: *Lunar and Planetary Science IX*, pp. 907–909.
- Plaut, J.J. et al., 2009. Radar evidence for ice in lobate debris aprons in the mid-northern latitudes of Mars. *Geophys. Res. Lett.* 36, L02203.
- Popova, O.P., Hartmann, W.K., Nemtchinov, I.V., Richardson, D.C., Berman, D.C., 2007. Crater clusters on Mars: Shedding light on martian ejecta launch conditions. *Icarus* 190, 50–73.
- Preblich, B.S., McEwen, A.S., Studer, D.M., 2007. Mapping rays and secondary craters from the martian crater Zunil. *J. Geophys. Res.* 112, E05S06.
- Robbins, S.J., Hynek, B.M., 2011. Secondary crater fields from 24 large primary craters on Mars: Insights into nearby secondary crater production. *J. Geophys. Res.* 116, E10003.
- Robbins, S.J., Hynek, B.M., 2012. A new global database of Mars impact craters ≥ 1 km: 2. Global crater properties and regional variations of the simple-to-complex transition diameter. *J. Geophys. Res.* 117, E06001.
- Schaller, E.L., Burray, B., Pathare, A.V., Ramussen, J., Byrne, S., 2005. Modifications of secondary craters on the martian south polar layered deposits. *J. Geophys. Res.* 110, E02004.
- Schorghofer, N., 2007. Dynamics of ice ages on Mars. *Nature* 449, 192–194.
- Schorghofer, N., Forget, F., 2012. History and anatomy of subsurface ice on Mars. *Icarus* 220, 1112–1120.
- Segura, T.L., Toon, O.B., Colaprete, A., Zahnle, K., 2002. Environmental effects of large impacts on Mars. *Science* 298, 1977–1980.
- Sejourne, A., Costard, F., Gargani, J., Soare, R.J., Marmo, C., 2012. Evidence of an eolian ice-rich and stratified permafrost in Utopia Planitia, Mars. *Planet. Space Sci.* 60, 248–254.
- Senft, L.E., Stewart, S.T., 2008. Impact crater formation in icy layered terrains on Mars. *Meteor. Planet. Sci.* 43, 1993–2013.
- Sizemore, H.G., Zent, A.P., Rempel, A.W., in press. Initiation and growth of martian ice lenses. *Icarus*, 10.
- Skinner, J.A., Hare, T.M., Tanaka, K., 2006. Digital renovation of the atlas of Mars 1:15,000,000-scale global geologic series map. *Lunar Planet. Sci.* XXXVII.
- Smith, P.H. et al., 2009. H₂O at the Phoenix landing site. *Science* 325, 58–61.
- Soare, R.J., Costard, F., Pearce, G.D., Sejourne, A., 2012. A re-interpretation of the recent stratigraphical history of Utopia Planitia, Mars: Implications for late-Amazonian periglacial and ice-rich terrain. *Planet. Space Sci.* 60, 131–139.
- Stepinski, T.F., Mendenhall, M.P., Bue, B.D., 2009. Machine cataloging of impact craters on Mars. *Icarus* 203, 77–87.
- Stuurman, C.M., Osinski, G.R., Brothers, T.C., Holt, J.W., Kerrigan, M., 2014. SHARAD reflectors in Utopia Planitia, Mars consistent with widespread, thick subsurface ice. *Lunar Planet. Sci. Conf.*, Abstract #2262, 45.
- Weiss, D.K., Head, J.W., 2013. Formation of double-layered ejecta craters on Mars: A glacial substrate model. *Geophys. Res. Lett.* 40, 3819–3824.
- Zahnle, K.J., Colaprete, A., 2007. Secondary craters and the liberation of ice on Mars. In: *Seventh International Conference on Mars*.
- Zanetti, M., Hiesinger, H., Reiss, D., Hauber, E., Neukum, G., 2010. Distribution and evolution of scalloped terrain in the southern hemisphere, Mars. *Icarus* 206, 691–706.